AGU PUBLICATIONS

Geophysical Research Letters

RESEARCH LETTER
10.1002/2015GL063180

Key Points:
- At same conditions, a releasing bend is easier to form than a restraining bend
- The results may help explain the formation of the Salton Sea pull-apart basin
- The results may help explain why releasing bends are more common

Supporting Information:
- Figures S1–S4

Correspondence to:
J. Ye and M. Liu,
jiyang.ye@mail.missouri.edu;
lium@missouri.edu

Citation:
Ye, J., M. Liu, and H. Wang (2015), A numerical study of strike-slip bend formation with application to the Salton Sea pull-apart basin, *Geophys. Res. Lett.*, *42*, doi:10.1002/2015GL063180.

Received 19 JAN 2015
Accepted 6 FEB 2015
Accepted article online 11 FEB 2015

A numerical study of strike-slip bend formation with application to the Salton Sea pull-apart basin

Jiyang Ye[1], Mian Liu[1], and Hui Wang[2]

[1]Department of Geological Sciences, University of Missouri, Columbia, Missouri, USA, [2]Institute of Earthquake Sciences, China Earthquake Administration, Beijing, China

Abstract How stepovers of strike-slip faults connect to form bends is a question important for understanding the formation of push-up ranges (restraining bends) and pull-apart basins (releasing bends). We investigated the basic mechanics of this process in a simple three-dimensional viscoelastoplastic finite element model. Our model predicts localized plastic strain within stepovers that may eventually lead to the formation of strike-slip bends. Major parameters controlling strain localization include the relative fault strength, geometry of the fault system, and the plasticity model assumed. Using the Drucker-Prager plasticity model, in which the plastic yield strength of the crust depends on both shear and normal stresses, our results show that a releasing bend is easier to develop than a restraining bend under similar conditions. These results may help explain the formation of the Salton Sea pull-apart basin in Southern California 0.5–0.1 Ma ago, when the stepover between the Imperial Fault and the San Andreas Fault was connected by the Brawley seismic zone.

1. Introduction

Strike-slip faults are usually complex systems that grow from connecting fault segments over stepovers to form bends [*Aydin and Nur*, 1982; *Cunningham and Mann*, 2007; *Mann*, 2007; *McClay and Bonora*, 2001; *Segall and Pollard*, 1980]. For a dextral strike-slip fault, a restraining bend may form at a left-stepover, whereas a releasing bend may form at the right-stepover (Figures 1a and 1b). How the faults connect stepovers to form bends is important for understanding the formation of pull-apart basins and push-up ranges [*Aydin and Nur*, 1982; *Mann*, 2007].

The formation of strike-slip bends from stepovers has been investigated in analogue models [*Cooke et al.*, 2013; *McClay and Bonora*, 2001; *Wu et al.*, 2009]. Analogue models are good at illustrating the growth history of bends, but they do not provide direct stress-strain information for understanding the underlying mechanics. Numerical models also have been used [*Petrunin and Sobolev*, 2008; *Segall and Pollard*, 1980; *Ten Brink et al.*, 1996]; for simplicity these models were limited to elastic rheology. However, plastic strain needs to be calculated to show where new faults may develop to connect stepovers to form bends [*Li et al.*, 2009; *Liu et al.*, 2010; *Petrunin and Sobolev*, 2008].

In this study, we investigated the basic mechanics of forming strike-slip bends from stepovers, using a simple three-dimensional (3-D) viscoelastoplastic finite element model. Our study is motivated by the formation of the Salton Sea pull-apart basin in Southern California (Figures 1c and 1d). Here the relative Pacific-North American plate motion is accommodated by the San Andreas Fault (SAF), the transform plate boundary, and numerous subparallel faults, including the Imperial Fault (IMF) and the San Jacinto Fault (SJF). Located at the stepover between the southern SAF and the IMF, the Salton Sea pull-apart basin developed in the past 0.5~0.1 Ma as the stepover is connected by the Brawley Fault [*Brothers et al.*, 2009; *Fuis and Mooney*, 1990], shown as an active seismic belt with recent earthquake swarms [*Hauksson et al.*, 2013; *Lohman and McGuire*, 2007] and moderate earthquakes [*Chu and Helmberger*, 2013; *Hauksson et al.*, 2013]. The Salton Sea region features high heat flow, low seismic velocity in the upper mantle [*Tape et al.*, 2009], active crustal extension [*Crowell et al.*, 2013], significant basin sedimentation [*Dorsey*, 2010], and active volcanism [*Schmitt and Vazquez*, 2006; *Schmitt et al.*, 2012], all typical to pull-apart basins [*Cunningham and Mann*, 2007]. We have conducted numerical experiments to investigate how strain localizes in the SAF-IMF and SJF-IMF stepovers, and particularly, why a pull-apart basin formed here instead of a push-up range, which would result from connecting the SJF-IMF stepover.

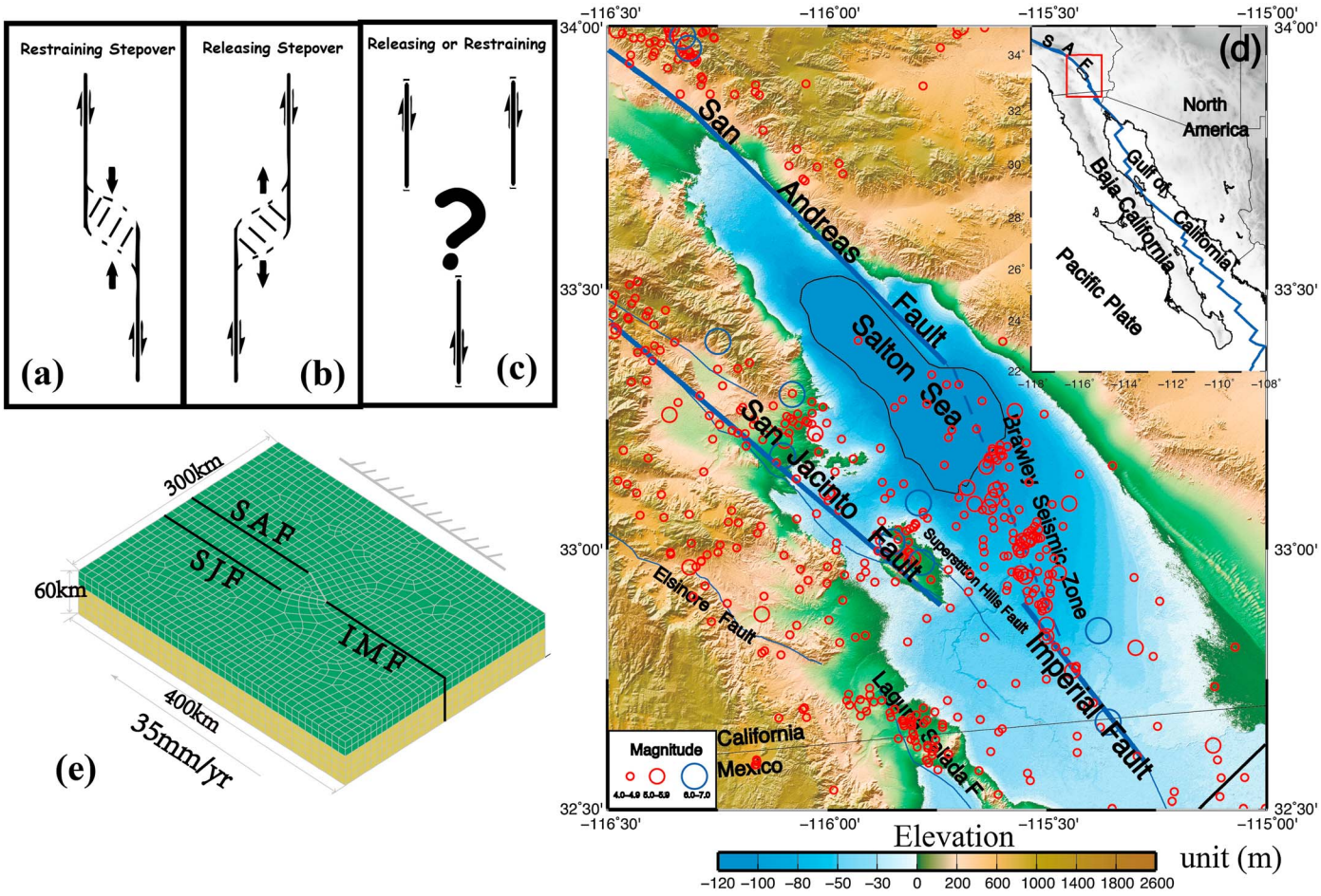

Figure 1. Sketch of (a) a restraining stepover that may grow into a push-up range in the hatched region, (b) a releasing stepover that may connect to form a pull-apart basin, and (c) a scenario where either a releasing or a restraining bend may develop. (d) Topographic relief, active faults (lines), and seismicity (circles) in the Salton Sea region. The inset map shows the regional tectonic setting of the study area (in box). (e) Mesh and boundary conditions of the finite element model. The black lines are strike-slip faults. SAF: the San Andreas Fault; SJF: the San Jacinto Fault; IMF: the Imperial Fault. The upper layer (green) represents the brittle (elastoplastic) upper crust and the lower layer (yellow) represents the viscoelastic lower crust and mantle. See text for details of rheology and boundary conditions.

2. Finite Element Model

We use a 3-D viscoelastoplastic finite element code developed by *Li et al*. [2009] in this study. This finite element model calculates plastic strain both in and outside the faults for a quasi-steady fault system; the predicted localization of plastic strain in the crust would indicate where the new faults may initiate [*Liu et al*., 2010].

Figure 1e shows the model setup. The model domain consists of an elastoplastic upper crust and viscoelastic lower crust and mantle. The faults are represented by a thin (1 km) layer of fault elements with a lower plastic yielding strength than that of the surrounding crust (see below). The northern and southern sides of the model domain are set as far-field traction free boundaries. The surface is also traction free, and the bottom is fixed in the vertical direction and traction free in horizontal direction. The eastern side of the model, set in the stable North American Plate, is fixed. The western side is loaded by a shear velocity of 35 mm/yr, reflecting the relative motion between the Pacific and the North American Plates in Southern California [*DeMets et al*., 1994]. In this model we ignored gravitational body force, assuming all deformation is driven by the relative plate motion [*Li et al*., 2009].

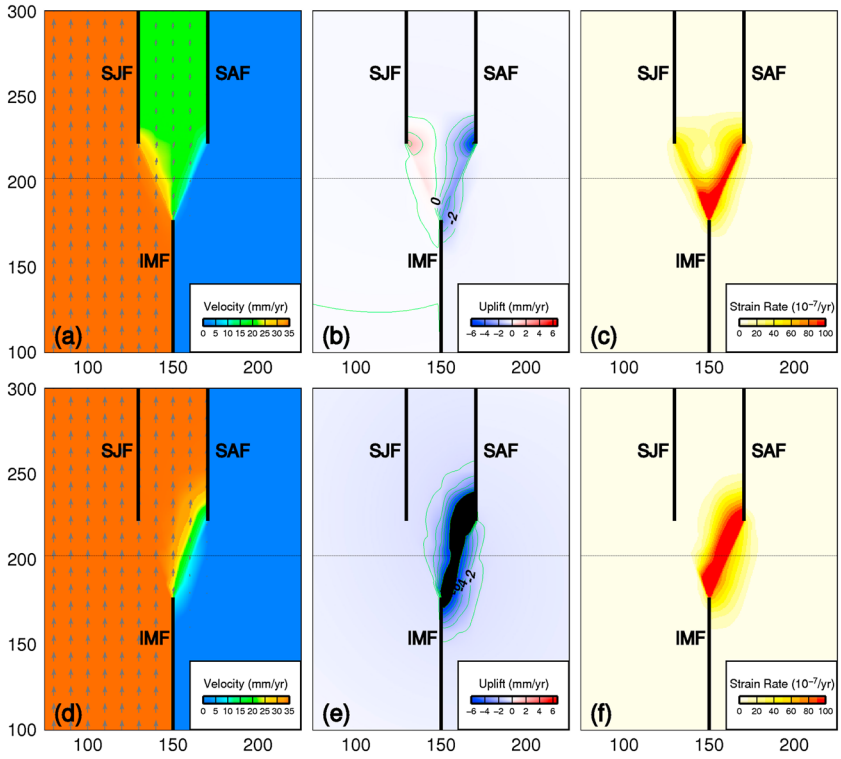

Figure 2. Predicted (a) horizontal and (b) vertical motions and (c) plastic strain rate for the reference case where all faults have the same strength. (d–f) Results for a case in which the SJF is taken to be 3 times stronger (measured in cohesion) than the SAF.

Under the imposed loading, the fault zones creep plastically when stress reaches the Drucker-Prager plasticity criteria [*Drucker and Prager*, 1952; *Li et al.*, 2009]. Similarly, plastic strain accumulates outside the fault zones where the stress reaches the plastic yield. For the upper crust outside the faults, the plastic strength is assigned through the values of cohesion (50 MPa) and internal frictional coefficient (0.4). For the fault zones, the cohesion is taken to be 10–30 MPa, and the internal frictional coefficient is set to zero, reflecting weak fault zones [*Bird and Kong*, 1994]. For the viscoelastic lower layer, we used viscosities in the range of 10^{19}–10^{21} Pa s; the elastic constants for the entire model domain are conventional values for the lithosphere: 8.75×10^{10} Pa for the Young's modulus and 0.25 for the Poisson's ratio [*Li et al.*, 2009; *Liu et al.*, 2010].

3. Model Results

To illustrate the basic mechanics of fault growth over stepovers, we started with a generic model motivated by the SAF-SJF-IMF fault system (Figure 1e), with same geometrical parameters for the SAF-IMF and SJF-IMF stepovers. Figures 2a–2c show the results of a model where all faults have the same strength. In this case, the simplified SJF and SAF each accommodated half the relative plate motion (Figure 2a). However, within the SAF-IMF stepover the motion is transtensional, resulting in subsidence, whereas it is transcompressive within the SJF-IMF stepover, causing uplift (Figure 2b). Although the fault geometry is symmetric, the predicted plastic strain rates are not: they are clearly concentrated within the SAF-IMF stepover (Figure 2c). The strain localization between the SAF-IMF would be enhanced if the SAF is weaker than the SJF (Figures 2d–2f), because the SAF is more mature than the young SJF [*Bird and Kong*, 1994; *Fay and Humphreys*, 2006].

These results suggest that a releasing bend may be easier to develop than a restraining bend when other conditions are the same. The reason is evident from the Drucker-Prager plasticity yield function: $F = \alpha I_1 + \sqrt{J_2'} - k$, where α and k are related to effective frictional coefficient and cohesion, respectively; I_1 is first invariant of the stress tensor, and J_2' is the second invariant of the deviatoric stress tensor. When lithostatic pressure is excluded, as often the case in geodynamic models, I_1 equals to the mean normal tectonic stress

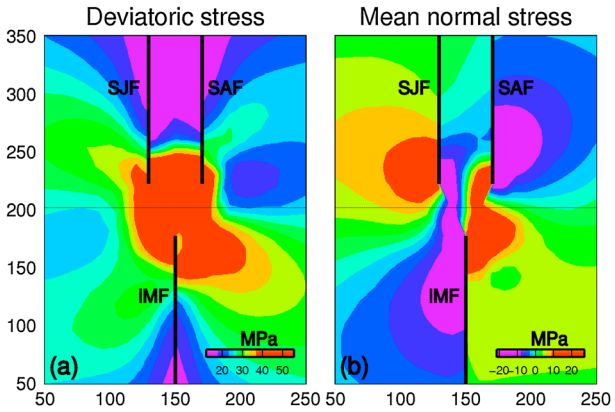

Figure 3. Predicted (a) deviatoric stress (the square root of the second invariant of the deviatoric stress tensor) and (b) the mean normal stress (compressional stress is negative) for the reference case where all faults have the same strength.

[*Li et al.*, 2009]. The parameter J_2' is related to shear stress. Thus, shear stress promotes plastic yield, whereas compressive (negative) mean normal stress has the opposite effects. Figure 3 shows the stress field assuming the same strength for all the faults. The shear stresses are similarly high within both the SAF-IMF and SJF-IMF stepovers (Figure 3a), but the mean normal stress is asymmetrically distributed: it is compressive (negative) around the SJF-IMF stepover, impeding plastic yield, but extensional (positive) around the SAF-IMF stepover, promoting plastic yield (Figure 3b). Hence, plastic strain tends to localized between the releasing stepover to form a releasing bend.

We adapted this model to the Salton Sea region, using the first-order fault geometry of the SAF, SJF, and IMF (Figure 4). Even assuming same strength for the SAF and SJF, the predicted plastic strain is localized in the SAF-IMF stepover, favoring the development of a pull-apart basin there. Stronger strain localization between the SAF-IMF stepover is predicted when the SAF is taken to be weaker than the younger SJF.

4. Discussion

We have shown that plastic strain tends to localize in gap of strike-slip stepovers, which may eventually grow into bends. Furthermore, strain localization is stronger in releasing stepovers than in restraining stepovers under similar conditions. The reason is the compressive mean normal stress between restraining stepovers and extensional mean normal stress between releasing stepovers. In the Drucker-Prager plasticity model or other plasticity models where plastic yield is a function of both mean normal and shear stresses, extensional mean normal stress promotes plastic yield, where compressive mean normal stress does the opposite. When we run the same model using the von Mises plasticity model, which assumes plastic yield depends only on the shear stress, strain is equally localized between releasing stepover and restraining stepover. We believe that the Drucker-Prager plasticity model is better suited for the upper crust, where plastic strain occurs mainly in the form of frictional sliding, and the yield strength increases with compressive normal stress [*Byerlee*, 1978].

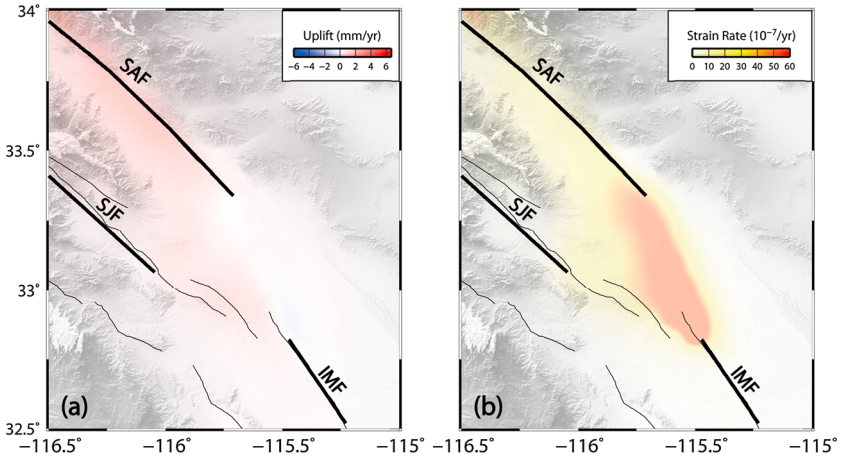

Figure 4. Predicted (a) vertical motion and (b) plastic strain rate for the Salton Sea region, assuming same strength for the San Andreas Fault (SAF) and the San Jacinto Fault (SJF).

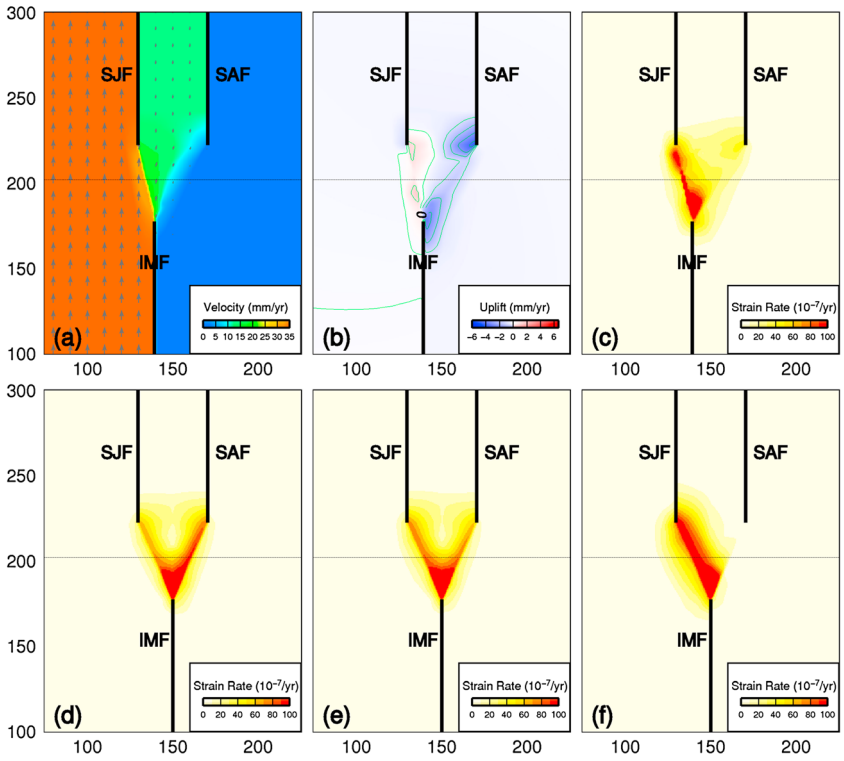

Figure 5. Effects of the width of the stepovers on the predicted (a) horizontal and (b) vertical motions and (c) plastic strain rate, for the case where the SJF-IMF stepover is 3 times narrower (measured as the distance between the trace of the faults) than the SAF-IMF stepover. The lower panels show the predicted plastic strain rate when the SAF is (d) 1.2 times, (e) 1.5 times, and (f) 3 times stronger than the SJF.

These results may explain, at least partially, why the number of recognized releasing bends is nearly 3 times that of restraining bends in the world's strike-slip fault systems [*Mann*, 2007]. In some cases, nature may not have the choice: if a dextral fault grows from a system of left stepovers, the only way to connect the fault segments is to form restraining bends. The geometry of stepovers and fault strength also matter. In Figure 5, we show that a restraining bend would result if we make the width of the restraining SJF-IMF stepover more than 3 times narrower than the releasing SAF-IMF stepover (Figures 5a–5c), or if we assume that the SJF is more than 1.5 times weaker than the SAF (Figures 5d–5f). Both cases, of course, are inconsistent with the SAF-SJF-IMF system; they are hypothetical to show some of the conditions that would allow restraining bend to grow over a potential releasing bend.

Our results may help explain the formation of the Salton Sea pull-apart basin, which has grown from connecting the SAF-IMF stepover by the Brawley Fault in the past 0.5–0.1 Ma [*Brothers et al.*, 2009; *Fuis and Mooney*, 1990]. Of course, this is not the only cause of the Salton Sea pull-apart basin, which is located in the Salton Trough, a broader extensional feature formed about 5 Ma [*Fuis et al.*, 1984; *Lachenbruch et al.*, 1985; *Parsons and McCarthy*, 1996]. The Salton Trough is suggested to be the northern extension of Gulf of California segment of the East Pacific Rise [*Biehler*, 1964; *Elders et al.*, 1972]. The associated lithospheric heating and magma intrusion during the formation of Salton Trough may have caused the lithosphere under the IMF-SAF stepover to be weaker than under the IMF-SJF stepover. Alternatively, the lithosphere in the Salton region may be weakened by mantle upwelling [*Elders et al.*, 1972; *Fay et al.*, 2008; *Lachenbruch et al.*, 1985] related to the spreading ridges in Gulf California [*Biehler*, 1964; *Elders et al.*, 1972]. To explore the effects of lithospheric weakening on the formation of the Salton Sea pull-apart basin, we compared two cases with the reference case shown in Figures 2a–2c. In these two cases, we put a weak zone (with reduced viscosity of the viscous lower layer by an order of 2) under one of the stepover. As expected, a weak zone under the SAF-IMF stepover increases the plastic strain there, helping the formation of the pull-apart basin (Figures S1a–S1c in the supporting information). Putting a similar weak zone under the SJF-IMF stepover,

however, does little to localize plastic strain there (Figure S1d). Hence, thermal weakening may not be the controlling factor for the formation of the Salton Sea pull-apart basin.

To illustrate the basic mechanics of bend growth from stepovers, we used simplified fault geometry. Including secondary faults in the model would certainly complicate the simple strain patterns we show for the Salton Sea region (Figure 4). For example, the Superstition Hill fault between the restraining SJF-IMF stepover (Figure 1) is marked by active seismicity, indicating a restraining bend is forming there. On the other hand, these secondary faults do not change the strain pattern in the Salton Sea region that is dominated by localized strain in the releasing SAF-IMF stepover. We run some extreme cases where the SJF-IMF is already connected by a fault, yet the predicted strain is still localized in the SAF-IMF stepover (Figure S2). Our models also show significant rotation of the maximum horizontal stress around the stepovers (Figures S3 and S4), but a full discussion of stress orientations are beyond the scope of this work.

Finally, our results suggest that the development of the Salton Sea pull-apart basin can be affected by the relative strength of the faults. *Bennett et al*. [2004] have suggested that the slip rate of SAF accelerated relative to that on the SJF since 0.09 Ma. This may further contribute to the formation of Salton Sea pull-apart basin around 0.5–0.1 Ma [*Brothers et al*., 2009], as our results show that higher slip rates on the SAF would cause stronger strain localization in the IMF-SAF stepover.

5. Conclusions

Using a three-dimensional viscoelastoplastic finite element model, we have explored the mechanics of forming strike-slip bends from stepovers. Our results show that relative motion across stepovers causes localized plastic strain in the stepovers, which may activate existing faults or initiate new faults to connect stepovers into bends. Furthermore, under similar conditions a releasing bend is easier to form than a restraining bend, assuming plastic yielding of the crust depends on both normal and shear stresses. This mechanism helps explain the formation of the Salton Sea pull-apart basin, where the Imperial Fault connected with the southern San Andreas Fault to form a releasing bend. Other factors favoring the development of the Salton Sea pull-apart basin includes the southern SAF being relatively weaker than the subparallel SJF, and a weaker lithosphere and mantle upwelling under the Salton Sea region.

Acknowledgments
We thank Huai Zhang for assisting with the code development and GRL Editor Andy Newman and three anonymous reviewers for their helpful comments. This work was supported by NSF grant EAR-0948620.

The Editor thanks three anonymous reviewers for their assistance in evaluating this paper.

References

Aydin, A., and A. Nur (1982), Evolution of pull-apart basins and their scale independence, *Tectonics*, *1*(1), 91–105, doi:10.1029/TC001i001p00091.

Bennett, R. A., A. M. Friedrich, and K. P. Furlong (2004), Codependent histories of the San Andreas and San Jacinto fault zones from inversion of fault displacement rates, *Geology*, *32*(11), 961–964, doi:10.1130/g20806.1.

Biehler, S. (1964), *Geophysical Study of the Salton Trough of Southern California*, Geol. and Planetary Sciences, California Institute of Technology, Pasadena, Calif.

Bird, P., and X. Kong (1994), Computer simulations of California tectonics confirm very low strength of major faults, *Geol. Soc. Am. Bull.*, *106*(2), 159–174.

Brothers, D. S., N. W. Driscoll, G. M. Kent, A. J. Harding, J. M. Babcock, and R. L. Baskin (2009), Tectonic evolution of the Salton Sea inferred from seismic reflection data, *Nat. Geosci.*, *2*(8), 581–584, doi:10.1038/ngeo590.

Byerlee, J. (1978), Friction of rocks, *Pure Appl. Geophys.*, *116*(4–5), 615–626.

Chu, R., and D. V. Helmberger (2013), Source parameters of the shallow 2012 Brawley earthquake, Imperial Valley, *Bull. Seismol. Soc. Am.*, *103*(2A), 1141–1147.

Cooke, M. L., M. T. Schottenfeld, and S. W. Buchanan (2013), Evolution of fault efficiency at restraining bends within wet kaolin analog experiments, *J. Struct. Geol.*, *51*, 180–192.

Crowell, B. W., Y. Bock, D. T. Sandwell, and Y. Fialko (2013), Geodetic investigation into the deformation of the Salton Trough, *J. Geophys. Res. Solid Earth*, *118*, 5030–5039, doi:10.1002/jgrb.50347.

Cunningham, W., and P. Mann (2007), Tectonics of strike-slip restraining and releasing bends, *Geol. Soc. London Spec. Publ.*, *290*(1), 1–12.

DeMets, C., R. G. Gordon, D. F. Argus, and S. Stein (1994), Effect of recent revisions to the geomagnetic reversal time scale on estimates of current plate motions, *Geophys. Res. Lett.*, *21*(20), 2191–2194, doi:10.1029/94GL02118.

Dorsey, R. J. (2010), Sedimentation and crustal recycling along an active oblique-rift margin: Salton Trough and northern Gulf of California, *Geology*, *38*(5), 443–446, doi:10.1130/g30698.1.

Drucker, D. C., and W. Prager (1952), Soil mechanics and plastic analysis or limit design, *Q. Appl. Math.*, *10*, 157–165.

Elders, W. A., R. W. Rex, P. T. Robinson, S. Biehler, and T. Meidav (1972), Crustal spreading in Southern California: The Imperial Valley and the Gulf of California formed by the rifting apart of a continental plate, *Science*, *178*(4056), 15–24, doi:10.1126/science.178.4056.15.

Fay, N., and E. Humphreys (2006), Dynamics of the Salton block: Absolute fault strength and crust-mantle coupling in Southern California, *Geology*, *34*(4), 261–264, doi:10.1130/g22172.1.

Fay, N. P., R. A. Bennett, J. C. Spinler, and E. D. Humphreys (2008), Small-scale upper mantle convection and crustal dynamics in Southern California, *Geochem. Geophys. Geosyst.*, *9*, Q08006, doi:10.1029/2008GC001988.

Fuis, G. S., and W. D. Mooney (1990), Lithospheric structure and tectonics from seismic-refraction and other data, in *The San Andreas Fault System, California*, *U.S. Geol. Surv. Prof. Pap.*, pp. 206–236, Washington, D. C.

Fuis, G. S., W. Mooney, J. Healy, G. McMechan, and W. Lutter (1984), A seismic refraction survey of the Imperial Valley region, California, *J. Geophys. Res.*, *89*(B2), 1165–1189, doi:10.1029/JB089iB02p01165.

Hauksson, E., J. Stock, R. Bilham, M. Boese, X. Chen, E. J. Fielding, J. Galetzka, K. W. Hudnut, K. Hutton, and L. M. Jones (2013), Report on the August 2012 Brawley earthquake swarm in Imperial Valley, Southern California, *Seismol. Res. Lett.*, *84*(2), 177–189.

Lachenbruch, A. H., J. Sass, and S. Galanis (1985), Heat flow in southernmost California and the origin of the Salton Trough, *J. Geophys. Res.*, *90*(B8), 6709–6736, doi:10.1029/JB090iB08p06709.

Li, Q., M. Liu, and H. Zhang (2009), A 3-D viscoelastoplastic model for simulating long-term slip on non-planar faults, *Geophys. J. Int.*, *176*(1), 293–306.

Liu, M., H. Wang, and Q. Li (2010), Inception of the eastern California shear zone and evolution of the Pacific-North American plate boundary: From kinematics to geodynamics, *J. Geophys. Res.*, *115*, B07401, doi:10.1029/2009JB007055.

Lohman, R. B., and J. J. McGuire (2007), Earthquake swarms driven by aseismic creep in the Salton Trough, California, *J. Geophys. Res.*, *112*, B04405, doi:10.1029/2006JB004596.

Mann, P. (2007), Global catalogue, classification and tectonic origins of restraining-and releasing bends on active and ancient strike-slip fault systems, *Geol. Soc. London Spec. Publ.*, *290*(1), 13–142.

McClay, K., and M. Bonora (2001), Analog models of restraining stepovers in strike-slip fault systems, *AAPG Bull.*, *85*(2), 233–260.

Parsons, T., and J. McCarthy (1996), Crustal and upper mantle velocity structure of the Salton Trough, southeast California, *Tectonics*, *15*(2), 456–471, doi:10.1029/95TC02616.

Petrunin, A. G., and S. V. Sobolev (2008), Three-dimensional numerical models of the evolution of pull-apart basins, *Phys. Earth Planet. Inter.*, *171*(1-4), 387–399, doi:10.1016/j.pepi.2008.08.017.

Schmitt, A. K., and J. Vazquez (2006), Alteration and remelting of nascent oceanic crust during continental rupture: Evidence from zircon geochemistry of rhyolites and xenoliths from the Salton Trough, California, *Earth Planet. Sci. Lett.*, *252*(3), 260–274.

Schmitt, A. K., A. Martin, D. F. Stockli, K. A. Farley, and O. M. Lovera (2012), (U-Th)/He zircon and archaeological ages for a late prehistoric eruption in the Salton Trough (California, USA), *Geology*, *41*(1), 7–10, doi:10.1130/g33634.1.

Segall, P., and D. D. Pollard (1980), Mechanics of discontinuous faults, *J. Geophys. Res.*, *85*(B8), 4337–4350, doi:10.1029/JB085iB08p04337.

Tape, C., Q. Liu, A. Maggi, and J. Tromp (2009), Adjoint tomography of the Southern California crust, *Science*, *325*(5943), 988–992, doi:10.1126/science.1175298.

Ten Brink, U. S., R. Katzman, and J. Lin (1996), Three-dimensional models of deformation near strike-slip faults, *J. Geophys. Res.*, *101*(7), 16,205–16,220, doi:10.1029/96JB00877.

Wu, J. E., K. McClay, P. Whitehouse, and T. Dooley (2009), 4D analogue modelling of transtensional pull-apart basins, *Mar. Pet. Geol.*, *26*(8), 1608–1623, doi:10.1016/j.marpetgeo.2008.06.007.

Geophysical Research Letter

Supporting Information for

A numerical study of strike-slip bend formation with application to the Salton Sea

Jiyang Ye[1§], Mian Liu[1§] and Hui Wang[2]

[1]Dept. of Geological Sciences, University of Missouri, Columbia, MO 65211, USA.

[2]Institute of Earthquake Sciences, China Earthquake Administration, Beijing 100036, China.

§ Corresponding author (jiyang.ye@mail.missouri.edu and lium@missouri.edu)

Contents of this file

Figures S1 to S4

Introduction

This supporting information contains four figures that are referenced in the main article as Fig. Sx.

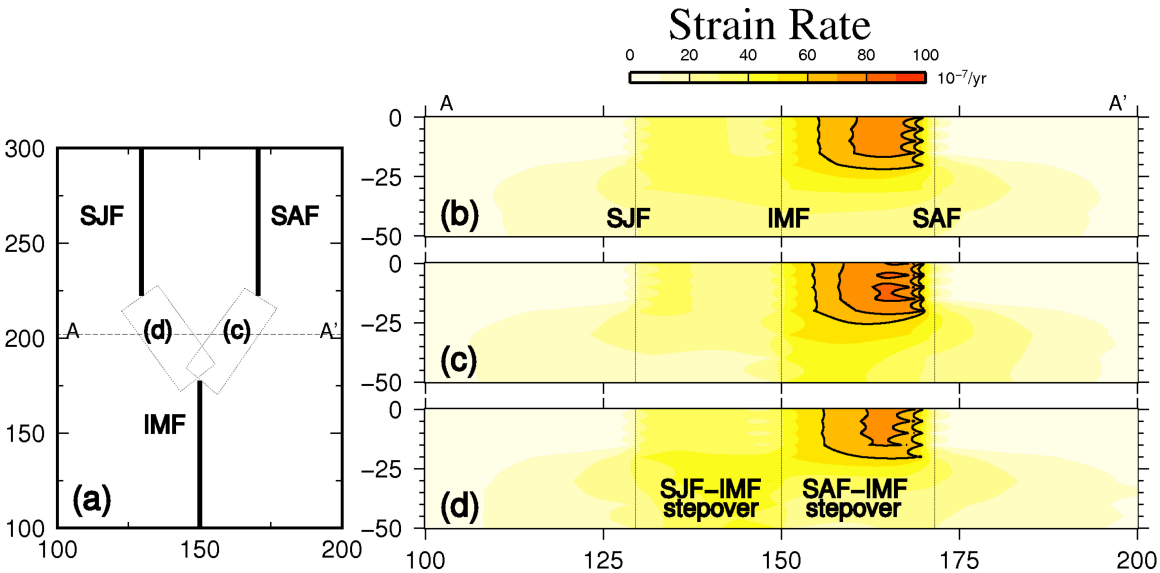

Figure S1. Effects of a weak zone in the lower crust and mantle. **(a)** Locations of the weak zones for results shown in (c) and (d). AA' shows the location of the vertical profiles in the right panels. **(b)** Predicted plastic strain rates for the reference case, where no weak zone under either stopover is assumed; **(c)** a weak zone is beneath the SAF-IMF stepover; **(d)** a weak zone is beneath the SJF-IMF stepover. Note that having a weak zone under the IMF-SJF does not cause the plastic strain to be preferably localized there.

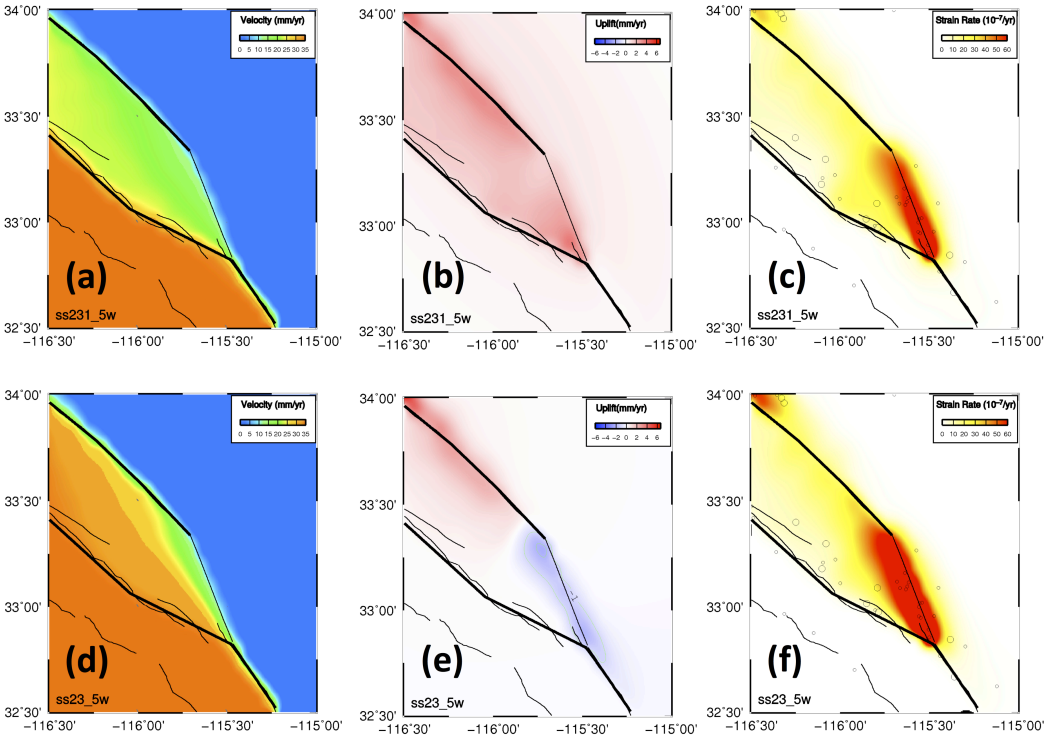

Figure S2. Two extreme cases show the impact of the Superstition Hill fault and other secondary faults in the SJF-IMF stepover. In two cases the SJF is assumed to be connected with IMF by theses secondary faults. Note that in both cases strain is still localized in the releasing SAF-IMF stepover. **(a-c)** Predicted horizontal motion, vertical motion, and plastic strain rate, respectively, assuming the same strength for all faults. **(d-f)** Results for a case in which the SJF is taken to be three times stronger (measured in cohesion) than the SAF.

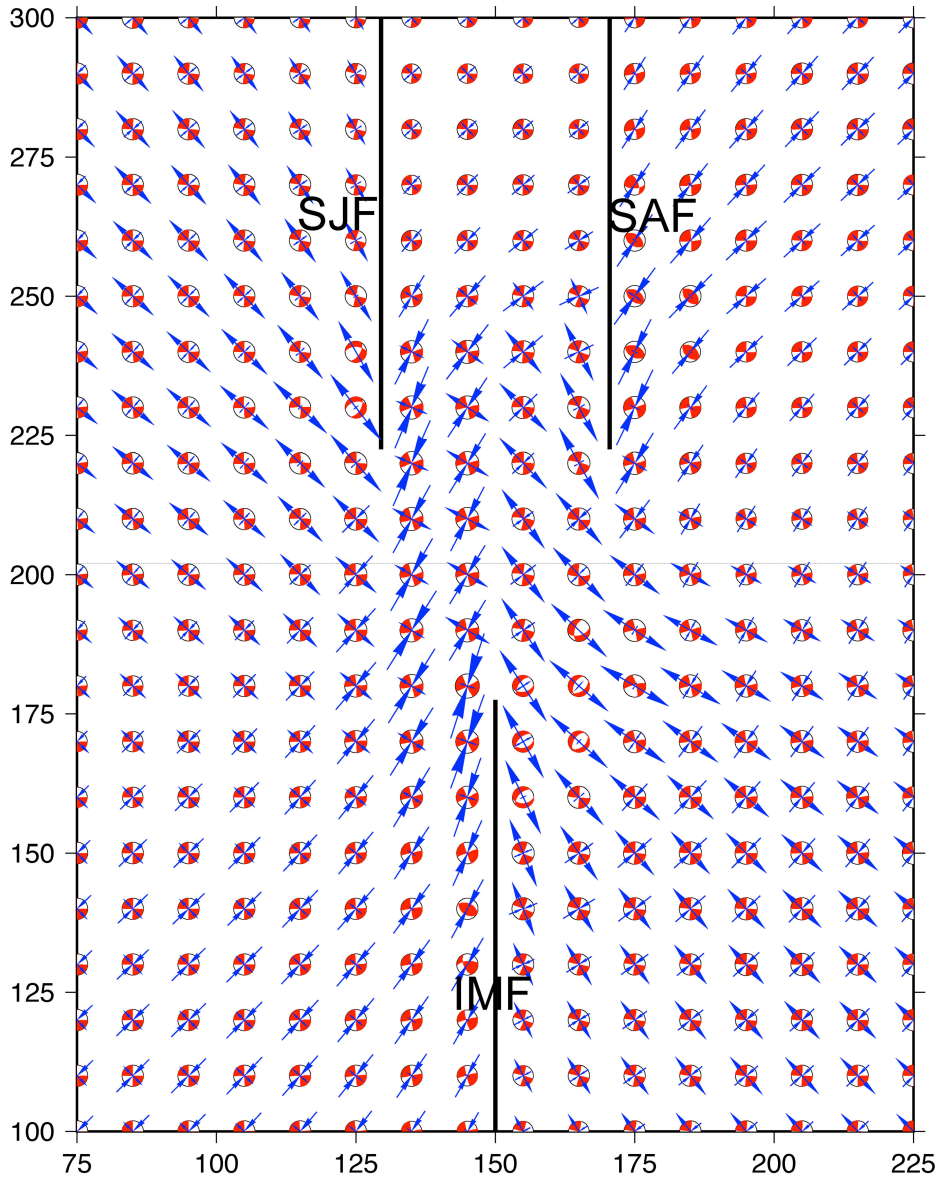

Figure S3. Model predicted principal stress field assuming the same fault strength for the SJF and SAF. The arrows show the horizontal maximal and minimal principal stresses. The "beach balls" show the 3-D principal stress state using the stereographic lower-hemisphere projection similar to that for earthquake focal mechanisms. The maximum (σ1) and minimum (σ3) principal stresses bisect the white and shaded quadrants, respectively, and are similar to the P- and T- axes in earthquake focal mechanisms.

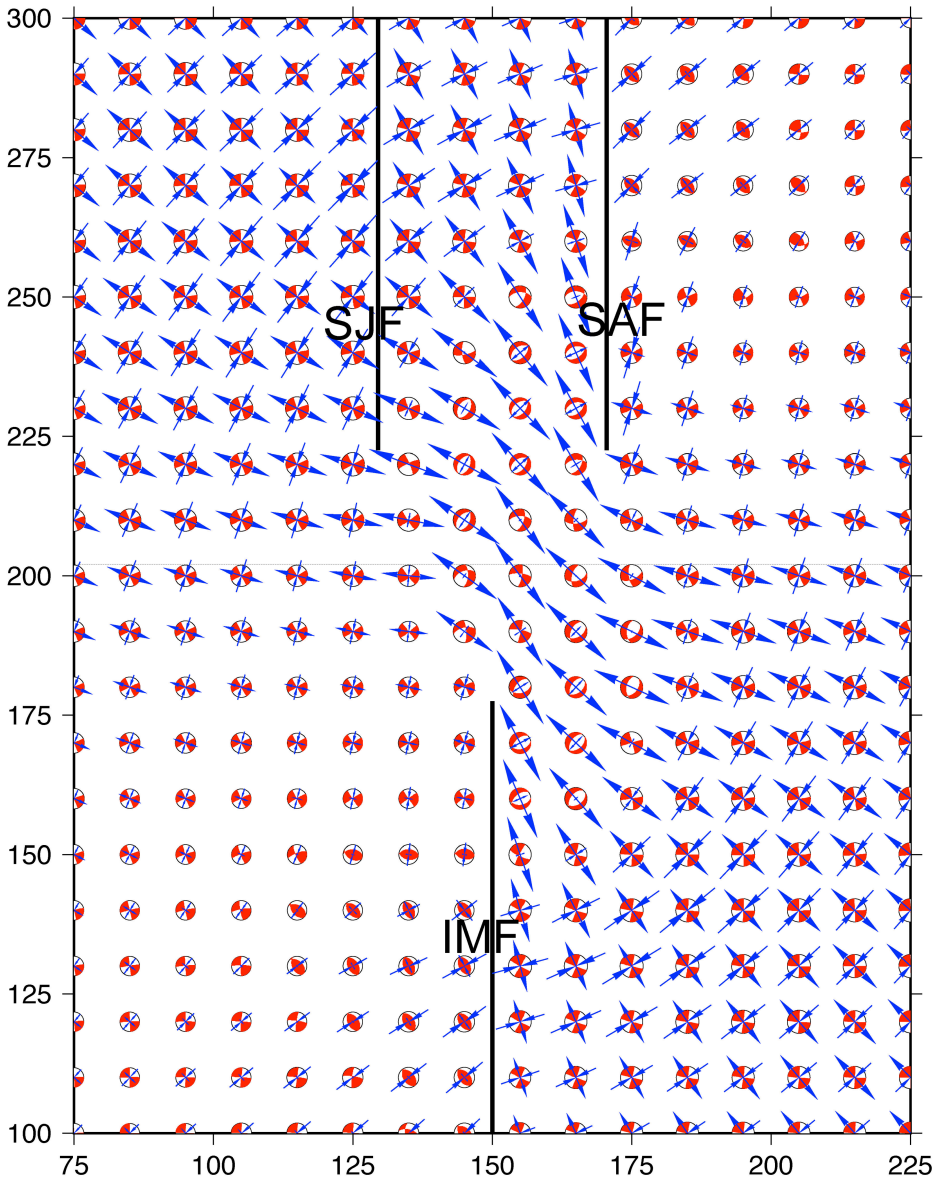

Figure S4. Predicted principal stress field for the case assuming the SJF to be 3 times stronger than SAF. The arrows show the horizontal maximal and minimal principal stress. The "beach balls" show the 3D principal stress state using the stereographic lower-hemisphere projection.